Silver-containing metallo hydrogel as a nanocatalyst for hydrogen evolution

Article

Accepted Version

Mondal, T., Patra, S. ORCID: https://orcid.org/0000-0003-4572-614X, Mondal, B., Ghosh, P. ORCID: https://orcid.org/0000-0002-2827-3313, Hamley, I. W. ORCID: https://orcid.org/0000-0002-4549-0926 and Banerjee, A. ORCID: https://orcid.org/0000-0002-1309-921X (2024) Silver-containing metallo hydrogel as a nanocatalyst for hydrogen evolution. ACS Applied Polymer Materials, 6 (18). pp. 11383-11391. ISSN 2637-6105 doi: 10.1021/acsapm.4c01965 Available at https://centaur.reading.ac.uk/118680/

Silver Containing Metallo Hydrogel as a Nanocatalyst for Hydrogen Evolution

Tanushree Mondal,[a] Suman Patra,[b] Biplab Mondal,[a] Purnadas Ghosh,[a] Ian W. Hamley,[c] and Arindam Banerjee*[a]

[a]School of Biological Sciences, Indian Association for the Cultivation of Science, A2A & 2B Raja S. C. Mullick Road, Jadavpur, Kolkata-700032

[b]School of Chemical Sciences, Indian Association for the Cultivation of Science, A2A & 2B Raja S. C. Mullick Road, Jadavpur, Kolkata-700032

[c]Department of Chemistry, University of Reading, Reading RG6 6AD, UK

*E-mail: bcab@iacs.res.in

Abstract: In recent years, non-noble metal catalysts for hydrogen evolution have drawn significant attention. Silver (Ag), is more abundant in the Earth's crust, relatively inexpensive, and exhibits excellent thermal and electrical conductivity compared to other noble metals, has rarely been considered as a potential electrocatalyst for hydrogen evolution. This piece of work demonstrates a tripeptide-based amphiphilic gelator forms metallo hydrogels in the presence of metal ions such as Ag^{+}, Ni^{2+}, or Co^{2+} in phosphate buffer at pH 7.46. The morphological studies of metallogels reveal the nanofibrillar network structure. The silver ion containing metallogel can be photoreduced to form a hydrogel infused with silver nanoparticles are confirmed by the TEM, XPS and XRD analysis. Interestingly, both the silver metallogel (Ag^{+}) and the silver nanoparticle (Ag^{0}) containing metallogel can catalyse hydrogen production from water. As a result this silver nanoparticle embedded nanofibers exhibit hydrogen evolution with an overpotential of 480 mV at a current density of 10

$mAcm^{-2}$ having a Tafel slope of 252 mV dec^{-1}, at a low electrochemical resistance in 0.5 M H_2SO_4 electrolyte, compared to other electrocatalysts under the same experimental conditions. Furthermore, this electrocatalyst has been witnessed to be highly stable during 2 h of chronoamperometric performance. This study highlights a promising avenue for utilizing a silver containing metallo hydrogel as a nanocatalyst for water splitting, offering a clean and sustainable method for generating hydrogen as a green energy resource.

Keywords: peptide • metallogel • self-assembly • HER •nanocatalyst

Introduction

Peptide-based low molecular weight hydrogelators (LMWHGs) continue to draw significant attention from researchers owing to their diverse structural and functional properties.[1-4] Supramolecular hydrogels arise from the hierarchical self-assembly of low molecular weight organic compounds through various non-covalent interactions, including hydrogen bonds[1], π–π stacking,[5] metal coordination,[6,7] and van der Waals forces.[3] These interactions create a three-dimensional architecture capable of arresting water molecules under appropriate conditions, resulting in the formation of hydrogels.[1,3,5] Supramolecular gels find extensive applications such as drug delivery,[8] wound healing,[9] antimicrobial agents,[3] oil spill recovery,[10] designing templates for nanohybrid systems,[1] and *in situ* formation and stabilization of nanoparticles.[11] Numerous studies have demonstrated that incorporation of metal cations can trigger self-assembly in water to form metallo hydrogels.[4,6] Peptides, with their diverse functional groups, offer a wide range of interactions with metal ions.[2,7] Metallogels are one of the supramolecular polymeric assembly accelerated by the metal-ligand coordination as well as other weaker noncovalent interactions. Peptides are eventually fabricated with various metal coordination sites such as –COOH and –OH groups which help the additional metal-ligand interactions.[7] This metal-ligand interactions can play a crucial role

for the fabrications of supramolecular polymeric gels containing metal ions which led to the development and fabricating of both soft and organic-inorganic composite materials.[12] These metal-bonded organic-inorganic composites find applications in various fields including metal ion triggered self-shrinking,[2,7] self-healing,[13] antimicrobial activity,[14] and catalytic activity.[15] Continuous depletion of fossil fuels and non-renewable resources have sparked widespread concern over the energy crisis. Given the increasing awareness of environmental challenges and the surge in energy requirements, the adoption of clean and renewable energy sources becomes imperative.[16] In response to this urgent challenge, hydrogen has emerged as a focal point of extensive research as an ideal and sustainable energy carrier.[17] Indeed, the exploration of cost-effective and eco-friendly hydrogen production is a significant challenge as traditional hydrogen production methods have economical drawbacks and environmental issues. In this era, among all hydrogen generation technologies, electrochemical water splitting stands out as a clean and efficient method for producing molecular hydrogen [H_2].[18,19] However, due to limitations in reaction kinetics, the hydrogen evolution reaction (HER) is sluggish. Consequently, there is a crucial need for a highly efficient electrocatalyst to accelerate the overall process. Extensive efforts have been undertaken to develop the efficient and cost-effective electrocatalysts to enhance the hydrogen production.[20,21] To date, most of the reported HER catalysts are mainly noble metal Pt-based electrocatalysts,[22] non-noble metal electrocatalysts,[23] and non-metal electrocatalysts.[19,24] Generally, Pt-based catalysts are the most promising for HER due to their prominent catalytic activity.[22,25] The major disadvantages are limited supply and high cost and due to these factors they are not applied for large scale commercialization. This motivates the development of non-noble metal based high-performance and inexpensive HER catalysts, significant research challenge.[26-39] Silver-based nanomaterials have drawn significant attention due to their exceptional electrical conductivity, plasmonic properties, and remarkable stability. This

makes them highly promising for catalytic applications.[40] In recent years, the fabrication of supramolecular metallogels using self-assembled moieties and 3D transition metals has become increasingly popular.[41] These self-assembled materials hold potential uses across various fields, including energy storage, optoelectronics, and energy conversion.[41,42] The versatility and robustness of these nanomaterials make them ideal for developing innovative solutions in a wide range of applications, emphasizing their role in the future of material science and engineering.[40-42] Despite extensive studies on heterogeneous catalysis, the use of peptide-based metallogels and organic-inorganic composite nanomaterials remains relatively unexplored. Supramolecular self-assembling nanomaterials are receiving significant attention due to their diverse applications in sustainable energy and environmental remediation.[43,44] These self-assembled systems present diverse opportunities for surface functionalization and facilitate environmentally friendly conditions for metal ion binding, leading to the formation of inorganic nanomaterials allowing for the fine-tuning of catalytic activity.[1] Moreover, the incorporation of nanomaterials into self-assembling systems has been shown to significantly enhance catalytic activity across various electrochemical processes.[45,46] The synthesis of metal nanoparticles (NPs) within a self-assembled gel phase offers the scope to prepare soft materials with embedded templated nanoparticle arrays.[11] Notably, the self-assembly of peptide molecules has successfully enabled the controlled arrangement in the synthesis of metallic nanoparticles (NPs) in the hydrogel matrix and used as an efficient electrocatalyst for HER.[45]

Experimental Section

Materials. Myristic acid (min 98% pure), L-tryptophan (ExiPlus, 99%), L-tyrosine (min 99%), DCC (99% pure), hydroxybenzotriazole (HOBt) (extrapure, min 99%), silica gel (100−200 mesh min 90%, Brockmann activity grade 2−3), chloroform, methanol, petroleum ether, ethyl acetate, THF, and DMF, $SOCl_2$, $NiCl_2.6H_2O$, $CoCl_2.6H_2O$, $AgNO_3$ were

purchased from SRL (India), 10% Pt/C purchased from Sigma Aldrich. All the solvents were pure, 99%. NaOH (NLT 97%) was acquired from Rankem. Nafion-117 solution was purchased from Sigma Aldrich Chemicals. Carbon cloth was obtained from Global Nanotech, Mumbai, India.

Synthesis and Characterization of amphiphilic Peptide (P1). In this work, we have synthesized an amphiphilic peptide containing L-tryptophan (W), L-tyrosine (Y) and a long fatty acyl chain myristic acid (C_{14}) i.e. C_{14}-W-Y-W-OH (P1) by conventional solution phase methods (Scheme S1) by using a racemization-free fragment condensation strategy. All steps of the synthetic details were provided in the Supporting Information. The final compound was fully characterized by mass spectrometry (Figure S1), ^{1}H NMR spectroscopy (Figure S2), and ^{13}C NMR spectroscopy (Figure S3). Comprehensive characterization of these metallogels are conducted using various techniques including Fourier-transform infrared spectroscopy (FT-IR), X-ray diffraction (XRD), rheology analysis, small-angle X-ray scattering (SAXS), and field emission gun transmission electron microscopy (FEG-TEM), Field emission scanning electron microscopy (FE-SEM). Additionally, the formation of silver nanoparticles was confirmed through UV spectroscopy, XRD, FEG-TEM, X-ray photoelectron spectroscopy (XPS), and selected area electron diffraction (SAED) experiments. This kind of synthesis of silver nanoparticles (AgNPs) by amphiphilic peptide has great interest owing to their ease of functionality. The catalytic activity for electrochemical hydrogen generation is studied by several electrochemical techniques such as linear sweep voltammetry (LSV), Tafel slope analysis and electrochemical impedance spectroscopy (EIS) by using aggregated solution of P1 (Gelator), Ag-Gel and AgNP-Gel as catalyst.

Preparation of metallo hydrogels [Co-Gel], [Ni-Gel], [Ag-Gel] and [AgNP-Gel] from peptide amphiphile. In the gelation study, 5 mg of peptide amphiphile was suspended in 1

mL of phosphate buffer at pH 7.46, resulting in a final concentration of 6.55 mM. To ensure a homogeneous solution, the sample underwent sonication for 5 minutes at room temperature, followed by gentle heating at 100 °C for 10 minutes. Despite these efforts, the transparent solution formed aggregates that did not transition into a hydrogel even after 24 hours. Subsequently, the aggregated solution was treated with 6.4 μL of $NiCl_2.6H_2O$ (0.5 M), 6.5 μL of $CoCl_2.6H_2O$ (0.5 M) and 6.4 μL of $AgNO_3$ (0.5 M) solutions leading to the formation of a white-coloured cobalt (Co-Gel), nickel (Ni-Gel) and silver metallogels (Ag-Gel). Remarkably, exposure of this Ag-Gel to sunlight for 30 minutes resulted in the nanoparticles by transforming silver ions Ag (I) to silver nanoparticles Ag (0) within the gel matrix. This reduction process caused a distinct change in the colour of the gel from white to brown.

Preparation of electrodes Gelator/CC, Ag-Gel/CC, and AgNP-Gel/CC. The catalyst modified bare carbon cloth (CC) (1 × 1 cm^2) was used as the working electrode. 5 mg of P1 was dispersed in glass vial containing 1 mL of phosphate buffer pH 7.46 and dissolved it by heat and sonication. 200 μL of above mixture was taken and 20 μL Nafion was added to this mixture and dropcast onto bare CC and kept for drying under high vacuum for 4 h and used this fabricated catalyst/CC in electrochemical studies. 5 mg of P1 was dispersed in glass vial containing 1 mL of phosphate buffer pH 7.46 and dissolved it by heat and sonication and 6.4 μL of $AgNO_3$ (0.5 M) was added and formed Ag-Gel, when Ag-Gel exposed to light it formed AgNP-Gel. 200 μL of Ag-Gel was taken and 20 μL Nafion was added to this Ag-Gel and 200 μL of AgNP-Gel was taken and 20 μL Nafion was added to this. Both those mixtures were dropcasted on the bare CC and kept for drying under high vacuum for 4 h and used this fabricated catalyst/CC in electrochemical studies. For comparison, the working electrode was also prepared using commercial Pt/C by maintaining 5 mg of Pt/C in glass vial containing 1 mL isopropanol. 200 μL of this solution was taken and 20 μL Nafion was added and the mixture was dropcasted on carbon cloth and kept for drying under high vacuum for 4 h and

used this fabricated catalyst/CC in electrochemical studies. The catalyst loading was calculated as follows: [(200 × 5)/1000] mg = 1 mg. The calculated catalyst loading nearly 1 mg/ cm^2. The resultant Ag loading on the electrode surface was 0.3 mg/cm^2.

Electrochemical measurements. Electrochemical hydrogen evolution reaction (HER) measurements were conducted on a three-electrode system using Pt and Ag/AgCl (saturated KCl) as the counter and reference electrodes, respectively. Gelator/CC, Ag-Gel/CC, and AgNP-Gel/CC were used as a working electrode. Before electrochemical analysis, all electrolytes were purged with N_2 for 0.5 h LSV curves were recorded in, 0.5 M H_2SO_4 (pH=0.3) at a scan rate of 10 mV s^{-1}. The electrochemical impedance spectroscopy (EIS) experiments were carried out in the frequency range of 0.1 Hz to 10^5 Hz. The bias used for EIS measurement was -0.45 V vs Ag/AgCl. Electrochemical Equivalence Circuit for the EIS studies were also provide for Gelator, Ag-Gel, and AgNP-Gel (Figure S4). The electrochemically active surface area (ECSA) was assessed by the double-layer capacitance (C_{dl}) quantised from CV curves at variable scan rates (10–100 mV s^{-1}). For 0.5 M H_2SO_4 electrolyte, the Ag/AgCl electrode (3 M KCl) was used as the reference electrode. All potential values of the HER were calibrated to a reversible hydrogen electrode (RHE) using the equation $E_{(RHE)} = [E_{(Ag/AgCl)} + (0.059 \times pH) + 0.197\ V]$, $[E^0_{Ag/AgCl} = 0.197\ V]$ in 0.5 M H_2SO_4.

Calculations of Faradaic yield (FY).

AgNP-Gel deposited carbon cloth (1cm^2) was subjected to an applied potential of -0.5 V versus RHE in a N_2-saturated 0.5 M H_2SO_4 aqueous solution, H_2 formation was observed in Gas Chromatography equipped with a thermal conductivity detector (GC-TCD). The process consumed 97.6 C of charge, resulting in the production of 10.4 mL of H_2, which was measured by water replacement in an inverted burette.

The Faradaic yield (FY) can be calculated using the formula:

FY % = [2 × amount of H_2 (mol) × 96500] / charge consumed during Chronoamperometry. Given that the total volume of H_2 produced was 10.4 mL, and the amount of H_2 can be calculated as 10.4 / 22400 = 4.7×10^{-4} mol, the FY of H_2 is:

FY of H_2 = (2 × 4.7×10^{-4} × 96500) / 97.6 = 91.8%.

Results and Discussion

In this work, we have synthesized an amphiphilic peptide containing L-tryptophan (W), L-tyrosine (Y) and a long fatty acyl chain myristic acid (C_{14}) i.e. C_{14}-W-Y-W-OH (P1). Gelation tests revealed that P1 itself does not form gel, but appears as an aggregated solution in phosphate buffer. Metallogels are formed at 1:2 (Metal: P1) ratio by entrapping metal (Co^{2+} or Ni^{2+} or Ag^{+}) ions inside the cross-linked nanofibrillar network structure in phosphate buffer at pH 7.46 (Figure 1). Upon exposure to sunlight, the white-coloured silver metallogel (Ag-Gel) underwent reduction, leading to the generation of a hydrogel infused with silver nanoparticles (AgNP-Gel) with a concomitant colour change from white to brown (Figure 1).This kind of synthesis of silver nanoparticles (AgNPs) by amphiphilic peptide has great interest owing to their ease of functionality. The metallogels were comprehensively characterized using various instrumental techniques. The catalytic activity for electrochemical hydrogen generation was studied using Ag-Gel and AgNP-Gel as catalysts.

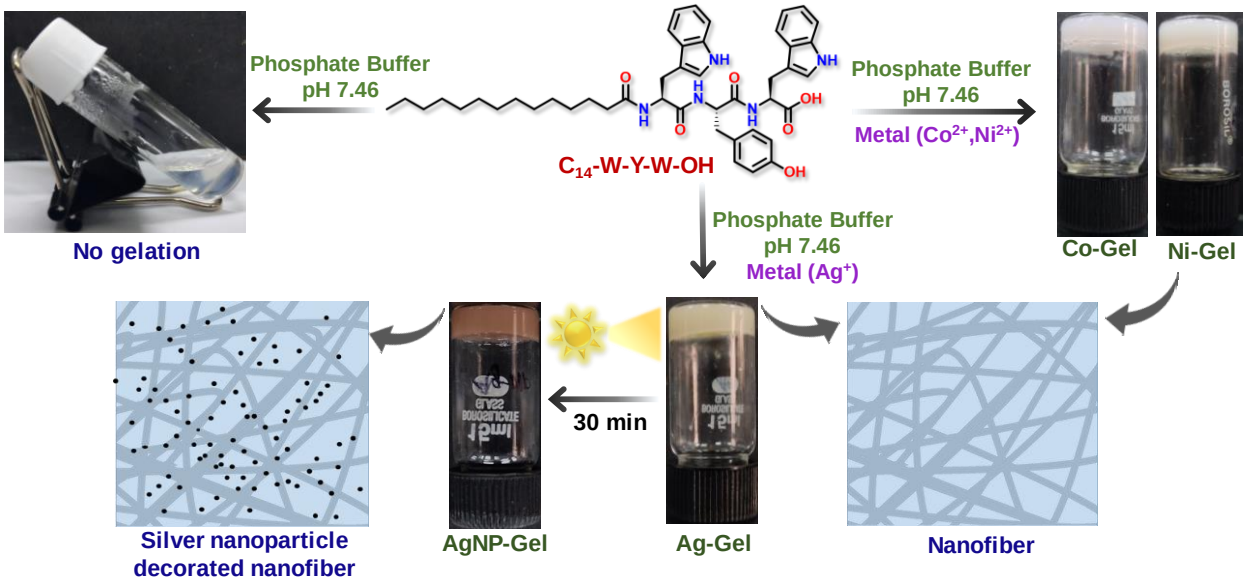

Figure 1. Schematic illustration of the formation of the peptide amphiphile based metallogels and silver nanoparticle-containing metallogels.

Fourier-transform infrared (FT-IR) spectroscopy is a powerful tool for identification of secondary structure of peptides. The amide I peak (1600-1700 cm^{-1}) in FT-IR spectra is associated with C=O stretching frequency and is centred at 1645, 1643, 1641, 1636 and 1636 cm^{-1} for gelator, Co-Gel, Ni-Gel, Ag-Gel and AgNP-Gel respectively (Figure S5a). The peaks centred at 3277-3286 cm^{-1} and 1535-1539 cm^{-1} correspond to the hydrogen bonding N–H stretching and bending frequencies, respectively.[45] Features at 3420-3425 cm^{-1} are due to non-hydrogen bonded N-H stretching.[3,45] Finally, the peaks in the ranges 2925-2930 cm^{-1} and 2851-2853 cm^{-1} are due to the asymmetric and symmetric stretching vibrations of CH_2 and CH_3, which indicates that the molecules have an all-trans configuration with a highly ordered structure.[3,7]

The colour change is the plasmonic characteristic of the AgNPs confirmed by the surface plasmon resonance (SPR) band between 400-500 nm in UV-Vis spectroscopy.[47] The absorption band of gelator and Ag-Gel appeared at 280 nm whereas, the absorption band for AgNP-Gel appeared at 280 nm and 450 nm (Figure S5b). The absorption band at 280 nm is due to tryptophan and tyrosine.[47] The peak at 450 nm is the characteristic of AgNPs due to SPR.[47] Tryptophan and tyrosine are the only aromatic amino acids that have unique photo physical and photochemical properties.[47] We also observed that white coloured silver metallogel was transformed to brown colour upon exposure to sunlight. The colour change is occurred due to the plasmonic characteristic of silver nanoparticles confirmed by the surface plasmon resonance band which is centred between 400–500 nm in UV-Vis spectroscopy,

revealing reduction of the Ag (I). When the tryptophan containing conjugates are exposed to sunlight, there is an electron transfer from tryptophan residue to Ag (I) ions, and this clearly reveals that Ag (I) ions interact with the Trp–Trp residue and accelerate the reduction process and it also confirms the formation of silver nanoparticle Ag (0).[47]

Powder X-ray diffraction (PXRD) analysis was performed to investigate the molecular packing and the supramolecular secondary structure adopted by the gelators in Ni-Gel, Co-Gel, Ag-Gel and AgNP-Gel. In the wide-angle X-ray diffraction pattern of the gelator, Ni-Gel, Co- Gel showed peaks at 4.75 Å (2θ = 18.16°), 4.84 Å (2θ = 18.20°) and 4.76 Å (2θ = 18.10°) corresponding to the distance between two β-strands.[3] The peaks at 3.87 Å (2θ = 22.33°), 3.75 Å (2θ = 23.02°), 3.69 Å (2θ = 22.40°) prove the presence of strong intermolecular π–π interactions between the aromatic groups of tryptophan and tyrosine (Figure 2a-c).[3] The XRD pattern confirms β-sheet formation by the gelator, Ni-Gel, and Co-Gel. The XRD study of Ag-Gel showed peaks at 4.73 Å (2θ =18.24°) and 3.84 Å (2θ = 22.48°) which correspond to the distances between two β-strands and intermolecular π–π interactions respectively (Figure 2d). AgNp-Gel showed peaks at 3.84 Å (2θ =22.50°) and 4.72 Å (2θ = 18.25°) for π–π stacking and β–sheet like structure respectively. Five peaks at 2θ values of 32.21° 38.03°, 44.32°, 64.71° and 77.52° correspond to (100) (111), (200), (220) and (311) reflections from silver nanoparticles (Figure 2e), having face centred cubic crystal structure.[48] This result indicates the *in situ* generation of AgNPs in the gel matrix.

To probe the mode of packing of the peptide amphiphile in the gel state, small-angle X-ray scattering (SAXS) was performed. The estimated molecular length of the peptide amphiphile is 21.84 Å. The d-spacing values were calculated from SAXS data to be 42.22 Å and 36.57 Å (Figure 2f) in Ag-gel. The d-spacing value of 42.22 Å is almost equal to double the molecular length indicating that two peptides amphiphile form a bilayer with coordination of the Ag^+ ion by the –COOH group. The d-spacing value 36.57 Å is longer than the length

of a single molecule (21.84 Å) and also and is less than double the molecular length, indicating interdigitated packing of the molecules. On the basis of SAXS and PXRD and FT-IR studies, a probable model for the molecular packing in the gel phase for the Ag-gel has been constructed (Figure S6).

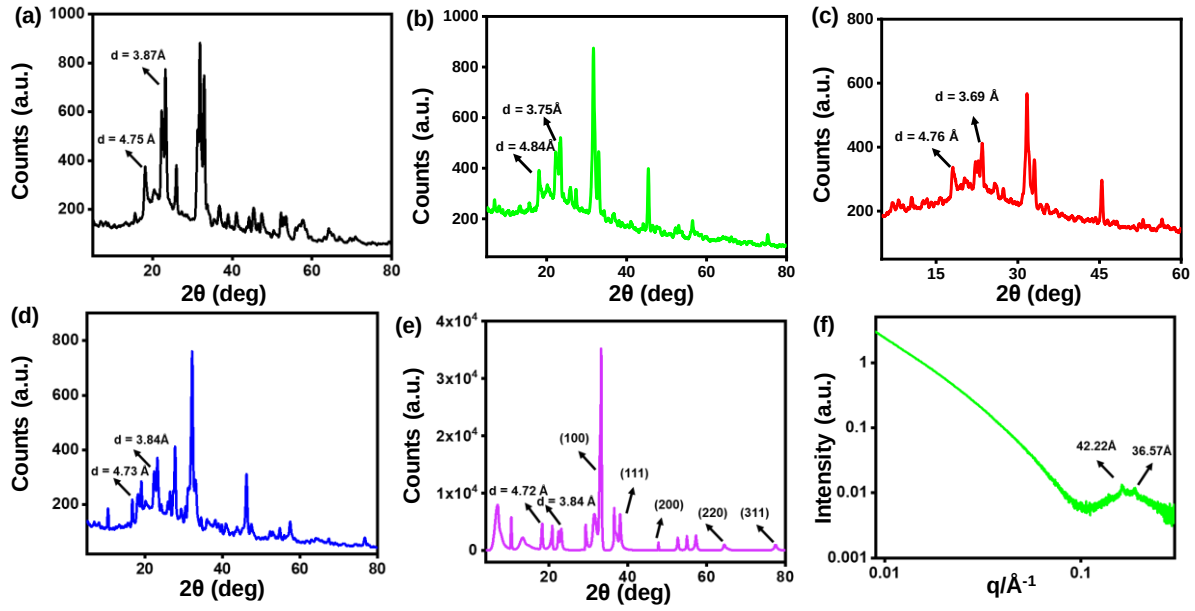

Figure 2. PXRD analysis of (a) Gelator, (b) Ni-Gel, (c) Co-Gel, (d) Ag-Gel (e) PXRD analysis of AgNP-Gel, (f) SASX analysis of Ag-gel.

Rheological experiments were carried out to determine the viscoelastic and mechanical properties of the hydrogel, when they are exposed to mechanical stress. The storage modulus (G') represents the elastic behaviour, and the loss modulus (G"), represents the viscous component of the flow. Two rheological experiments were carried out for Co-Gel, Ni-Gel, Ag-Gel and AgNP-Gel at 25°C: (i) frequency sweep experiment performed at a constant strain 0.1 % by varying the frequency 1 to 100 rad/s (Figure S7a-d) respectively.(ii) strain sweep experiment at a constant frequency 10 rad/s by varying the strain from 0.01 to 100 % (Figure S8a-d) respectively. At a constant strain of 0.1% and a fixed concentration of 0.5% w/v, the individual metallogels Co-Gel, Ni-Gel, Ag-Gel and AgNP-Gel show storage moduli

of 4.84×10^2 Pa, 1.87×10^2 Pa and 18.84×10^2 Pa and 5.34×10^2 Pa respectively at angular frequency (ω) = 100 rad/s. The moduli show an insignificant dependence on angular frequency, which indicates the formation of stable metallogel for Ag-Gel. But the storage modulus drops significantly AgNP-Gel. The reduction of mechanical strength of the gel due to nanoparticle formation has been reported.[11] The probable reason is that AgNPs are fabricated along the gel nanofibers and interact with the gelator network influencing fibril junction formation. This may lead to lower cross-link density, and a less uniform distribution, causing a significant reduction in gel strength.

The formation of AgNPs in the gel matrix was further confirmed by X-ray photoelectron spectroscopy (XPS). The XPS survey profile of AgNP-Gel confirms the presence of C, O, N and Ag (Figure 3a). The core level of Ag 3d spectrum (Figure 3b) shows two major peaks at 368.6 and 374.6 eV, corresponding to Ag $3d_{5/2}$ and Ag $3d_{3/2}$, respectively. The difference between the peak positions is 6 eV, indicating silver is present as silver nanoparticle Ag (0) in the gel matrix.[48,49] The core level XPS profile of C 1s (Figure 3c) shows deconvoluted peaks at 284.6, 285.6 and 288.3 eV attributed to the existence of C=C/ C=O, C−C/ C−O and O=C−OH bonding interactions respectively, present in the peptide amphiphile.[48] The high-resolution O 1s (Figure 3d) profile shows peaks at 530.5, 531.5 and 533.4 eV attributed to the presence of Ag−O, C=O and C–O bonding interactions.[48] The deconvoluted N 1s spectrum (Figure 3e) shows a peak at 399.9 eV which corresponds to C−N−C bonding interaction.[48]

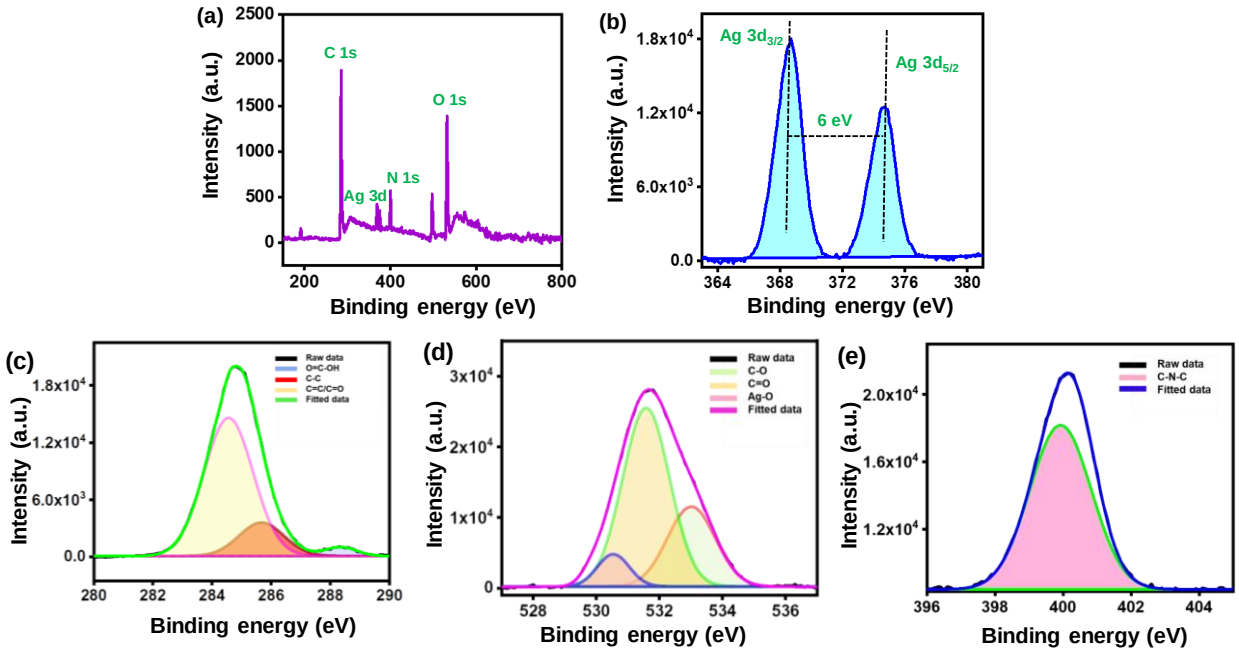

Figure 3. (a) XPS survey spectrum, (b) XPS spectrum of Ag 3d. AgNP-Gel with the high-resolution XPS profiles of (c) C 1s, (d) O 1s, and (e) N 1s.

Field emission gun transmission electron microscopy (FEG-TEM) was employed to examine the morphology of Co-Gel, Ni-Gel, Ag-Gel and AgNP-Gel. A nanofibrous assembly is evident for the gel of P1 (Figure 4a) where the fibers exhibit an average width of 20−25 nm. The Ag-Gel also displays a nanofibrous structure with fibers having an increased average width of 30−50 nm (Figure 4b). Upon exposure to sunlight, TEM observations reveal the formation of homogeneously decorated silver nanoparticles (AgNPs) along the fibrous network of Ag-Gel (Figure 4c).[50] Remarkably, the fibers maintain their nanofibrous morphology with an average width reduced to 10−15 nm (Figure 4c). This observation suggests that the AgNPs formed without compromise the integrity of the nanofibrous structure. Moreover, the TEM images indicate that the AgNPs aggregate along the nanofibers during the formation process. Size distribution and mean size analysis of the nanoparticles were conducted by randomly measuring nanoparticles from the FEG-TEM image. The majority of the AgNPs exhibit an average particle diameter ranging from 10 to 12 nm (Figure 4d), arranged in an array along the nanofibers. This comprehensive analysis provides valuable insights into the morphological transformations of gel fibers and the subsequent formation of AgNPs in the Ag-Gel system under exposure to sunlight. The Co-Gel and Ni-Gel revealed a nanofibrous assembly, where the fibers exhibited an average width of 22−25 nm, (Figure S9a,b). The crystallinity of silver nanoparticle was investigated by selected area electron diffraction (SAED). Interplanar spacing determined from the rings of the SAED patterns showing the plane distances 0.234, 0.203, 0.144, and 0.126 nm correspond to hkl

values of (111), (200), (220), and (311), respectively, confirmed the formation of fcc silver lattice (Figure S9c,d).[48,51]

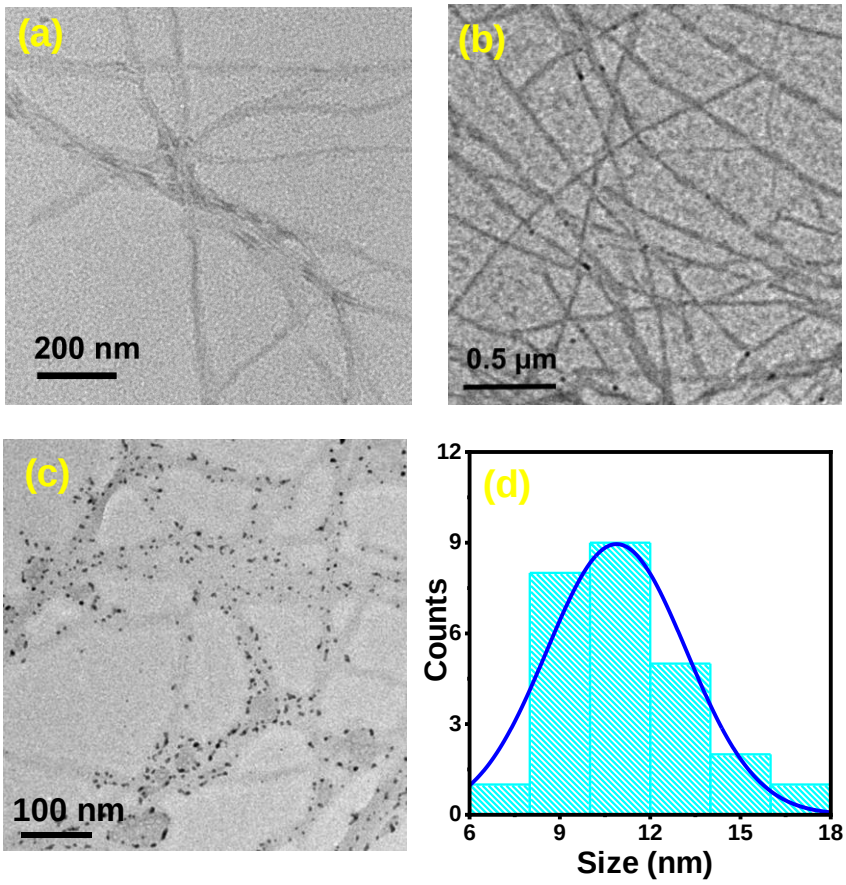

Figure 4. FEG-TEM images of the (a) Gelator, (b) Ag-Gel, (c) AgNP-Gel and (d) Size distribution histogram of silver nanoparticle in the gel matrix.

FE-SEM analysis was conducted to examine the surface morphology of various working electrodes: bare carbon cloth (CC) as a control, Gelator/CC, Ag-Gel/CC, and AgNP-Gel/CC, prior to the catalytic study (Figure 5). The carbon fibers on the bare carbon cloth displayed a smooth surface (Figure 5a). Upon drop-casting the catalysts, a homogeneous catalyst layer formed on the surface of the carbon cloth (Figure 5b-d).

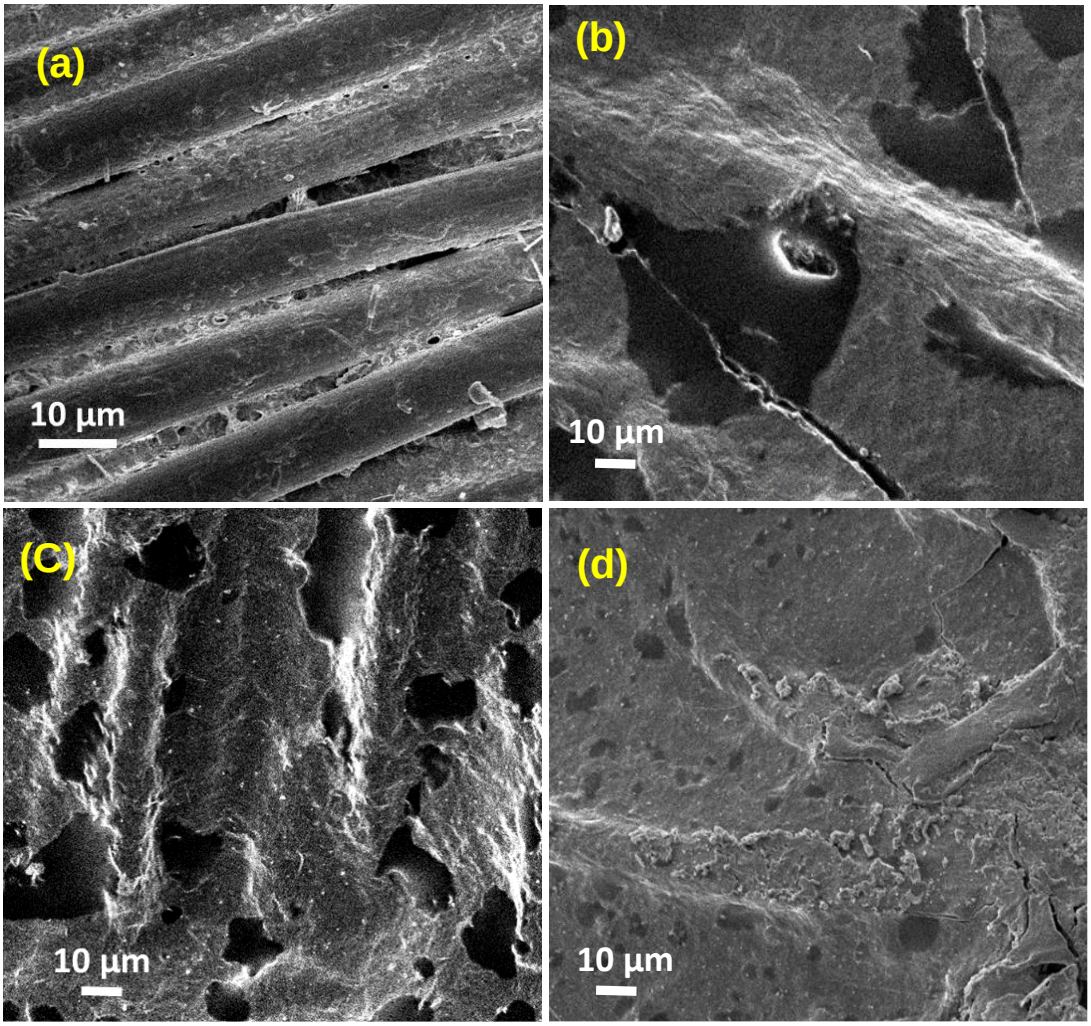

Figure 5. FE-SEM image of (a) Carbon cloth (control), (b) Gelator (c) Ag-Gel, (d) AgNP-Gel coated carbon cloth before electrochemical studies.

An initial assessment of HER activity for the P1 gelator, Ag-Gel, and AgNP-Gel was performed, using linear sweep voltammetry (LSV) conducted in 0.5 M H_2SO_4 solution (pH = 0.3) with a scan rate of 10 mV s^{-1}. Notably, AgNP-Gel exhibits an overpotential requirement of 480 mV to achieve a current density of 10 mA/cm^2, while Ag-Gel and gelator require larger overpotentials of 650 mV and 760 mV, respectively, for the same current density (Figure 6a). LSV was performed for the commercial Pt/C, used as a benchmark catalyst on

the carbon cloth surface and showed overpotential value 130 mV for the same current density and same experimental condition. The commercial Pt/C exhibited the lowest overpotential, demonstrating its excellent catalytic performance. Analysis of charge transfer kinetics at the electrode–electrolyte interface was performed using Tafel plots derived from LSV data. Pt/C displays a lower Tafel slopes of 195 mV dec^{-1} indicating faster charge transfer kinetics and (Figure 6b) AgNP-Gel displays a Tafel slopes 252 mV dec^{-1} comparatively lower than Ag-Gel (285 mV dec^{-1}), gelator (301 mV dec^{-1}) and carbon cloth (382 mV dec^{-1}). Electron transfer kinetics were further investigated through electrochemical impedance spectroscopy (EIS) (Figure 6c). AgNP-Gel exhibits a lower charge transfer resistance (R_{ct}) of 15.1 Ω compared to gelator (24.6 Ω) and Ag-Gel (17.5 Ω), indicating enhanced catalytic activity and faster charge transfer for AgNP-Gel (Table S1). This lower R_{ct} value suggests that the AgNP-Gel possesses a favourable structure for charge transfer and good electrical conductivity during HER. The electrochemical active surface area (ECSA) values were determined from double-layer capacitance (C_{dl}) data by using the equation: ECSA = (C_{dl}/C_s) where the C_s represents the capacitance value of the flat electrode surface and the value of C_s is equal to 0.04 mF/cm^2.[18] The scan rate-dependent CV curves are shown in (Figure S10a-c) for the gelator, Ag-Gel and AgNP-Gel respectively. From the slope of the given current density Δj vs. scan rate plot (Figure 6d), the C_{dl} values lead to ECSA values 12.19 cm^2, 46.5 cm^2, and 77 cm^2, for the gelator, Ag-Gel And AgNP-Gel respectively. This indicates that AgNP-Gel has a significantly higher exposed surface area for H^+ ion adsorption, facilitating hydrogen evolution.[52,53] Faradaic efficiency was determined by collecting the gaseous product into an inverted burette by vertical displacement of water and calculating the amount of charge consumed (Figure S11a) (91.8 %). The durability of the catalyst (AgNP-Gel) was evaluated through chronoamperometric (CPE) studies over 2 hours with a constant applied voltage of -0.5 V vs RHE potential (Figure S11b). The production of H_2 gas in the reaction chamber is

also confirm by the GC-TCD (Gas Chromatography-Thermal Conductivity Detector) analysis by measuring the produced gas under the application of a constant potential (Figure S12a).

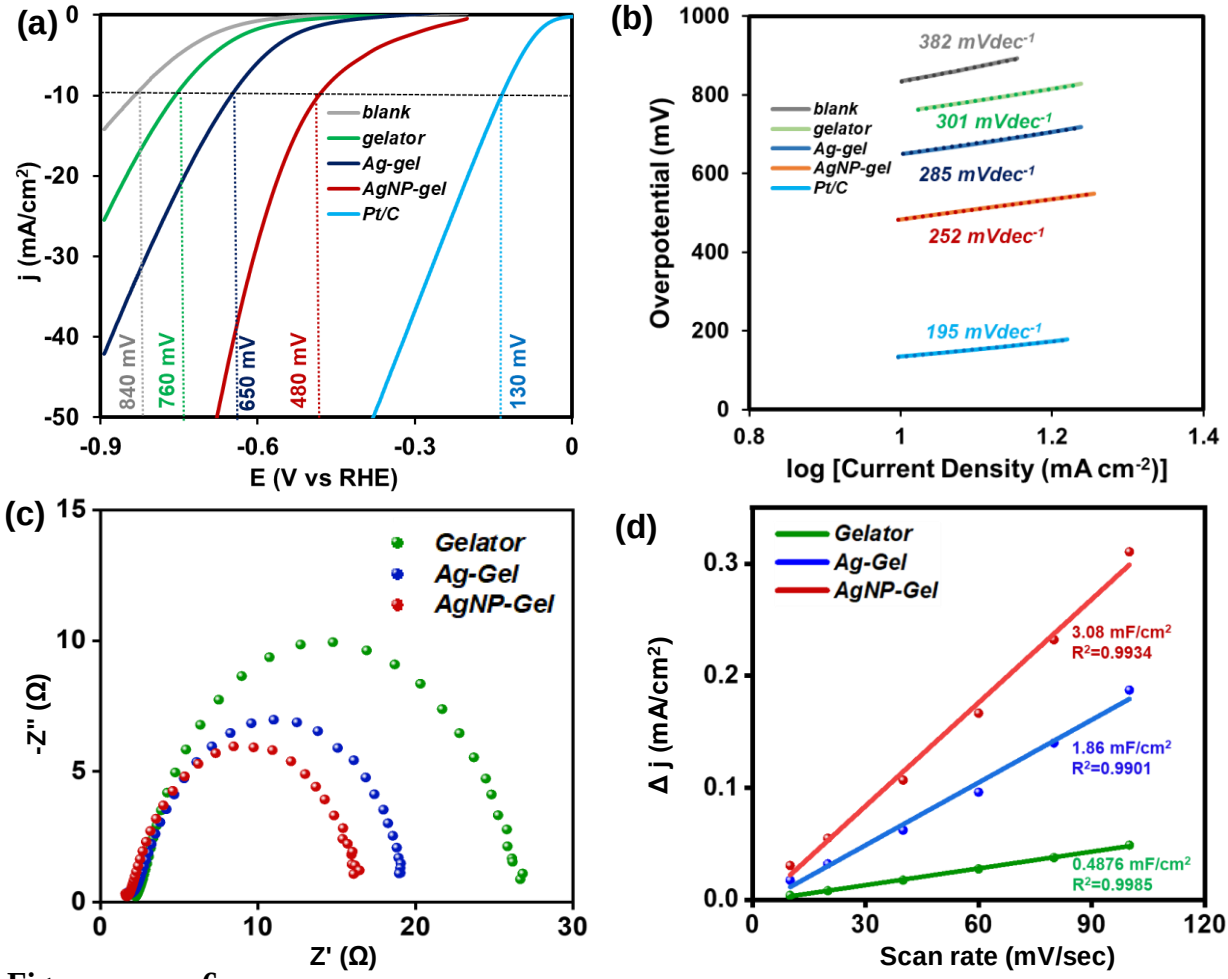

Figure 6. Electrochemical performance of the catalysts (a) Linear Sweep Voltametry curves (b) Tafel slopes (c) Nyquist plots (d) linear fit for double layer capacitance of the catalysts.

The post-catalytic stability of the catalyst was investigated using PXRD, FE-SEM, and FEG-TEM techniques. PXRD data of the used catalyst revealed that all the characteristic peaks, such as π–π stacking and β–sheet, remained unchanged after the catalytic reaction (Figure S13a-c) for the gelator, Ag-Gel, and AgNP-Gel. The peaks for silver nanoparticles at 2θ values of 32.21°, 38.03°, 44.32°, 64.71°, and 77.52°, corresponding to the (100), (111), (200), (220), and (311) planes, were also present after electrolysis. FE-SEM images for the

gelator, Ag-Gel, and AgNP-Gel before and after electrolysis indicated no change in morphology (Figure 5 and Figure S14). FEG-TEM analysis showed that the fiber-like morphology was retained for the gelator and Ag-Gel (Figure S15a,b). The morphological analysis of AgNP-Gel post-electrolysis also confirmed the presence of silver nanoparticles decorating the gel fibers (Figure S15c). Collectively, these post-electrolysis studies indicate that the catalysts remain structurally and morphologically unchanged after electrolysis. This stability is critical for ensuring consistent catalytic performance and reliability in subsequent catalytic cycles.

Conclusions

This study demonstrates the formation of metallo-hydrogels derived from a peptide amphiphile and metal cations including $Co^{2+,}$ Ni^{2+}or Ag^{+} in phosphate buffer pH 7.46. The remarkable transformation of a silver ion-containing gel upon sunlight exposure is noted, leading to the formation of Ag nanoparticle containing hydrogel. TEM studies clearly indicate the presence of self-assembled peptide nanofibers and the decoration of Ag nanoparticles on these fibers suggesting the formation of a nanohybrid system. The hydrogel based nanohybrid system acts as a catalyst for hydrogen evolution through water splitting at room temperature. Interestingly, these results clearly demonstrate the use of a peptide based nanohybrid system as a catalyst for the generation of renewable, clean and sustainable energy through hydrogen evolution.

Associated Content

Supporting Information

Synthetic scheme, synthetic procedure, FT-IR, UV, Rheology, FEG-TEM analysis, SAED pattern, CV plot, HR-MS data, ^{1}H and ^{13}C NMR data.

Notes

The authors declare no conflict of interest.

Acknowledgements

The authors want to acknowledge Prof. Abhishek Dey (IACS, India) and the CH instruments (CH 700E electrochemical analyser). The authors are also grateful to Prof. Asim Bhaumik and Sayantan Chongdar (IACS, India) for technical assistance in electrochemical instruments. T.M., S.P., P.G. wish to acknowledge Council of Scientific & Industrial Research (CSIR-India); B.M. acknowledges IACS for support.

References:

1. Paul, S.; Basu, K.; Das, K. S.; Banerjee, A. Peptide-Based Hydrogels as a Scaffold for *In situ* Synthesis of Metal Nanoparticles: Catalytic Activity of the Nanohybrid System. *ChemNanoMat* **2018**, *4*, 882–887.

2. Garcia, A. M.; Kurbasic, M.; Kralj, S.; Melchionna, M.; Marchesan, S. A Biocatalytic and Thermoreversible Hydrogel from a Histidine-Containing Tripeptide. *Chem. Commun.* **2017**, *53*, 8110–8113.

3. Mondal, T.; Chatterjee, A.; Hansda, B.; Mondal, B.; Sen, P.; Banerjee, A. Cationic and Amphiphilic Peptide-Based Hydrogels with Dual Activities as Anticancer and Antibacterial Agents. *Soft Matter* **2024**, *20*, 1236–1244.

4. Elsawy, M. A.; Wychowaniec, J. K.; Castillo Díaz, L. A.; Smith, A. M.; Miller, A. F.; Saiani, A. Controlling Doxorubicin Release from a Peptide Hydrogel through Fine-Tuning of Drug–Peptide Fiber Interactions. *Biomacromolecules* **2022**, *23*, 2624–2634.

5. Raeburn, J.; Adams, D. J. Multicomponent Low Molecular Weight Gelators. *Chem. Commun.* **2015**, *51*, 5170–5180.

6. Feldner, T.; Häring, M.; Saha, S.; Esquena, J.; Banerjee, R.; Díaz, D. D. Supramolecular Metallogel That Imparts Self-Healing Properties to Other Gel Networks. *Chem. Mater.* **2016**, *28*, 3210–3217.

7. Chen, J.; Wang, T.; Liu, M. A Hydro-Metallogel of an Amphiphilic L -Histidine with Ferric Ions: Shear-Triggered Self-Healing and Shrinkage. *Inorg. Chem. Front.* **2016**, *3*, 1559–1565.

8. Kumar, V. B.; Ozguney, B.; Vlachou, A.; Chen, Y.; Gazit, E.; Tamamis, P. Peptide Self-Assembled Nanocarriers for Cancer Drug Delivery. *J. Phys. Chem. B* **2023**, *127*, 1857–1871.

9. Yamada, Y.; Patel, N. L.; Kalen, J. D.; Schneider, J. P. Design of a Peptide-Based Electronegative Hydrogel for the Direct Encapsulation, 3D Culturing, in Vivo Syringe-

Based Delivery, and Long-Term Tissue Engraftment of Cells. *ACS Appl. Mater. Interfaces* **2019**, *11*, 34688–34697.

10. Mondal, B.; Bairagi, D.; Nandi, N.; Hansda, B.; Das, K. S.; Edwards-Gayle, C. J. C.; Castelletto, V.; Hamley, I. W.; Banerjee, A. Peptide-Based Gel in Environmental Remediation: Removal of Toxic Organic Dyes and Hazardous Pb^{2+} and Cd^{2+} Ions from Wastewater and Oil Spill Recovery. *Langmuir* **2020**, *36*, 12942–12953.

11. Nanda, J.; Adhikari, B.; Basak, S.; Banerjee, A. Formation of Hybrid Hydrogels Consisting of Tripeptide and Different Silver Nanoparticle-Capped Ligands: Modulation of the Mechanical Strength of Gel Phase Materials. *J. Phys. Chem. B* **2012**, *116*, 12235−12244.

12. Dey, S.; Misra, R.; Saseendran, A.; Pahan, S.; Gopi, H. N. Metal-Coordinated Supramolecular Polymers from the Minimalistic Hybrid Peptide Foldamers. *Angew. Chemie* **2021**, *133*, 9951–9956.

13. Häring, M.; Díaz, D. D. Supramolecular Metallogels with Bulk Self-Healing Properties Prepared by *in situ* Metal Complexation. *Chem. Commun.* **2016**, *52*, 13068–13081.

14. Lepcha, G.; Pal, B.; Majumdar, S.; Ahmed, K. T.; Pal, I.; Biswas, S. R.; Ray, P. P.; Dey, B. Ni(II) and Zn(II)-Metallogel-Based Anti-Bacterial Scaffolds for Fabricating Light-Responsive Junction-Type Semiconducting Diodes with Non-Ohmic Conduction Mechanism. *Mater. Adv.* **2023**, *4*, 2595–2603.

15. Slavík, P.; Kurka, D. W.; Smith, D. K. Palladium-Scavenging Self-Assembled Hybrid Hydrogels – Reusable Highly-Active Green Catalysts for Suzuki–Miyaura Cross-Coupling Reactions. *Chem. Sci.* **2018**, *9*, 8673–8681.

16. Danish, M. S. S. Exploring Metal Oxides for the Hydrogen Evolution Reaction (HER) in the Field of Nanotechnology. *RSC Sustain.* **2023**, *1*, 2180–2196.

17. Aparna, R. K.; Karmakar, A.; Arsha, R. T.; Kundu, S.; Mandal, S. Copper Nanoparticle-Embellished Zr-Based Metal–Organic Framework for Electrocatalytic Hydrogen Evolution Reaction. *Chem. Commun.* **2023**, *59*, 10444–10447.

18. Muhamed, S.; Aparna, R. K.; Karmakar, A.; Kundu, S.; Mandal, S. Immobilization of Gold Nanoparticles on Postsynthetically Modified NU-1000 for Hydrogen Evolution Reaction. *Inorg. Chem.* **2023**, *62*, 7195–7202.

19. Sadhukhan, A.; Karmakar, A.; Koner, K.; Karak, S.; Sharma, R. K.; Roy, A.; Sen, P.; Dey, K. K.; Mahalingam, V.; Pathak, B.; Kundu, S.; Banerjee, R. Functionality Modulation Toward Thianthrene-based Metal-Free Electrocatalysts for Water Splitting. *Adv. Mater.* **2024**, *36*, 1–13.

20. Rajput, A.; Pandey, A. A.; Kundu, A.; Chakraborty, B. Redox-Active Sn(II) to Lead to $SnFe_2O_4$ Spinel as a Bi-Functional Water Splitting Catalyst. *Chem. Commun.* **2023**, *59*, 4943–4946.

21. Sun, J.; Tian, F.; Yu, F.; Yang, Z.; Yu, B.; Chen, S.; Ren, Z.; Zhou, H. Robust Hydrogen-Evolving Electrocatalyst from Heterogeneous Molybdenum Disulfide-Based Catalyst. *ACS Catal.* **2020**, *10*, 1511–1519.

22. Shi, Y.; Ma, Z.-R.; Xiao, Y.-Y.; Yin, Y.-C.; Huang, W.-M.; Huang, Z.-C.; Zheng, Y.-Z.; Mu, F.-Y.; Huang, R.; Shi, G.-Y.; Sun, Y.-Y.; Xia, X.-H.; Chen, W. Electronic Metal–Support Interaction Modulates Single-Atom Platinum Catalysis for Hydrogen Evolution Reaction. *Nat. Commun.* **2021**, *12*, 3021–3033.

23. Bajpai, R.; Roy, S.; Verma, S. Microwave-Assisted Solid-State Synthesis of Dichalcogenide Nanostructures for Electrocatalytic Hydrogen Evolution. *ACS Appl. Nano Mater.* **2022**, *5*, 8511–8525.

24. Pradhan, A.; Manna, R. N. Surface-Modified Covalent Organic Polymer for Metal-Free Electrocatalytic Hydrogen Evolution Reaction. *ACS Appl. Polym. Mater.* **2021**, *3*, 1376–1384.

25. Fang, S.; Zhu, X.; Liu, X.; Gu, J.; Liu, W.; Wang, D.; Zhang, W.; Lin, Y.; Lu, J.; Wei, S.; Li, Y.; Yao, T. Uncovering Near-Free Platinum Single-Atom Dynamics during Electrochemical Hydrogen Evolution Reaction. *Nat. Commun.* **2020**, *11*, 1029.

26. Jiang, D.; Xu, Y.; Yang, R.; Li, D.; Meng, S.; Chen, M. CoP_3 /CoMoP Heterogeneous Nanosheet Arrays as Robust Electrocatalyst for PH-Universal Hydrogen Evolution Reaction. *ACS Sustain. Chem. Eng.* **2019**, *7*, 9309–9317.

27. Li, J.; Wang, R.; Dong, Z.; Zhang, X.; Li, X.; Li, Y.; Su, Z. Postdecorated Polyoxometalate Metal–Organic Framework-Constructed Ternary Electrocatalysts for Hydrogen Evolution. *Cryst. Growth Des.* **2023**, *23*, 6403–6409.

28. Li, J.-S.; Zhang, S.; Sha, J.-Q.; Wang, H.; Liu, M.-Z.; Kong, L.-X.; Liu, G.-D. Confined Molybdenum Phosphide in P-Doped Porous Carbon as Efficient

Electrocatalysts for Hydrogen Evolution. *ACS Appl. Mater. Interfaces* **2018**, *10*, 17140–17146.

29. Panda, C.; Menezes, P. W.; Yao, S.; Schmidt, J.; Walter, C.; Hausmann, J. N.; Driess, M. Boosting Electrocatalytic Hydrogen Evolution Activity with a $NiPt_3$@NiS Heteronanostructure Evolved from a Molecular Nickel–Platinum Precursor. *J. Am. Chem. Soc.* **2019**, *141*, 13306–13310.

30. Chongdar, S.; Ghosh, A.; Bal, R.; Bhaumik, A. Microwave-Assisted Synthesis of ZIF-9@ x GO Composites as Cooperative Electrocatalysts for Electro-Oxidation of Benzyl Alcohols Coupled with H_2 Production. *J. Mater. Chem. A* **2024**, *12*, 233–246.

31. Alharbi, T. M. D.; Elmas, S.; Alotabi, A. S.; Andersson, M. R.; Raston, C. L. Continuous Flow Fabrication of MoS_2 Scrolls for Electrocatalytic Hydrogen Evolution. *ACS Sustain. Chem. Eng.* **2022**, *10*, 9325–9333.

32. Aslan, E.; Sarilmaz, A.; Ozel, F.; Hatay Patir, I.; Girault, H. H. Catalytic Hydrogen Evolution by Molybdenum-Based Ternary Metal Sulfide Nanoparticles. *ACS Appl. Nano Mater.* **2019**, *2*, 7204–7213.

33. Csernica, P. M.; McKone, J. R.; Mulzer, C. R.; Dichtel, W. R.; Abruña, H. D.; DiSalvo, F. J. Electrochemical Hydrogen Evolution at Ordered Mo_7Ni_7. *ACS Catal.* **2017**, *7*, 3375–3383.

34. Ji, Z.; Trickett, C.; Pei, X.; Yaghi, O. M. Linking Molybdenum–Sulfur Clusters for Electrocatalytic Hydrogen Evolution. *J. Am. Chem. Soc.* **2018**, *140*, 13618–13622.

35. Mckone, J. R.; Sadtler, B. F.; Werlang, C. A.; Lewis, N. S.; Gray, H. B. Ni − Mo Nanopowders for Efficient Electrochemical Hydrogen Evolution. *ACS Catal*. **2013,** *3*, 166−169.

36. Mujtaba, J.; He, L.; Zhu, H.; Xiao, Z.; Huang, G.; Solovev, A. A.; Mei, Y. Co_9S_8 Nanoparticles for Hydrogen Evolution. *ACS Appl. Nano Mater.* **2021**, *4*, 1776–1785.

37. Ojha, K.; Saha, S.; Banerjee, S.; Ganguli, A. K. Efficient Electrocatalytic Hydrogen Evolution from MoS_2-Functionalized Mo_2N Nanostructures. *ACS Appl. Mater. Interfaces* **2017**, *9*, 19455–19461.

38. Sahoo, L.; Devi, A.; Patra, A. Atomically Precise Ni Nanoclusters for Improving Hydrogen Evolution Reaction Performance. *ACS Sustain. Chem. Eng.* **2023**, *11*, 4187–4196.

39. Tiwari, A. P.; McBride, S.; Hamlin, A. B.; Rahman, M. S.; Huddy, J. E.; Hautier, G.; Scheideler, W. J. MXene Anion Engineering for Efficient Hydrogen Evolution. *ACS Sustain. Chem. Eng.* **2023**, *11*, 12084–12092.

40. Kuo, T.-R.; Lee, Y.-C.; Chou, H.-L.; M G, S.; Wei, C.-Y.; Wen, C.-Y.; Chang, Y.-H.; Pan, X.-Y.; Wang, D.-Y. Plasmon-Enhanced Hydrogen Evolution on Specific Facet of Silver Nanocrystals. *Chem. Mater*. **2019**, *31*, 3722–3728.

41. Kwon, H.; Bae, D.; Won, D.; Kim, H.; Kim, G.; Cho, J.; Park, H. J.; Baik, H.; Jeong, A. R.; Lin, C.-H.; Chiang, C.-Y.; Ku, C.-S.; Yang, H.; Cho, S. Nanoporous Silver Telluride for Active Hydrogen Evolution. *ACS Nano* **2021**, *15*, 6540–6550.

42. Shokhen, V.; Kostikov, Y.; Borge-Durán, I.; Gershinsky, Y.; Grinberg, I.; Nessim, G. D.; Zitoun, D. Scalable Silver Oxo-Sulfide Catalyst for Electrochemical Water Splitting. *ACS Appl. Energy Mater.* **2019**, *2*, 788–796.

43. Gong, C.; Sun, S.; Zhang, Y.; Sun, L.; Su, Z.; Wu, A.; Wei, G. Hierarchical Nanomaterials via Biomolecular Self-Assembly and Bioinspiration for Energy and Environmental Applications. *Nanoscale* **2019**, *11*, 4147–4182.

44. Pelin, J. N. B. D.; Edwards-Gayle, C. J. C.; Castelletto, V.; Aguilar, A. M.; Alves, W. A.; Seitsonen, J.; Ruokolainen, J.; Hamley, I. W. Self-Assembly, Nematic Phase Formation, and Organocatalytic Behavior of a Proline-Functionalized Lipopeptide. *ACS Appl. Mater. Interfaces* **2020**, *12*, 13671–13679.

45. Kori, D. K. K.; Jadhav, R. G.; Dhruv, L.; Das, A. K. A Platinum Nanoparticle Doped Self-Assembled Peptide Bolaamphiphile Hydrogel as an Efficient Electrocatalyst for the Hydrogen Evolution Reaction. *Nanoscale Adv.* **2021**, *3*, 6678–6688.

46. Paul, S.; Banerjee, A. Stimuli Responsive Multicolour Fluorescence Emission in Carbon Nanodots and Application in Metal Free Hydrogen Evolution from Water. *Nanoscale Adv.* **2021**, *3*, 611–617.

47. Mishra, N. K.; Kumar, V.; Joshi, K. B. Thermoplasmonic Effect of Silver Nanoparticles Modulates Peptide Amphiphile Fiber into Nanowreath-like Assembly. *Nanoscale* **2015**, *7*, 20238–20248.

48. Ghosh, P.; Bairagi, D.; Hazra, N.; Jana, S.; Banerjee, A. Carbon-Dot-Decorated Silver and Gold Nanocomposites for Antibacterial Activity and Degradation of Organic Dyes. *ACS Appl. Nano Mater.* **2023**, *6*, 18100–18112.

49. Ghosh, P.; Hazra, S.; Gayen, K.; Hazra, N.; Nandi, A. K.; Banerjee, A. Peptide-Appended Perylene Bisimide Containing Silver Nanoparticle-Based Trihybrid System with GO: Improvement of Photocatalytic and Photo-Switching Behaviour. *New J. Chem.* **2024**, *48*, 9805–9813.

50. Bose, P.; Roy, J.; Khokhar, V.; Mondal, B.; Natarajan, G.; Manna, S.; Yadav, V.; Nyayban, A.; Yamijala, S. S. R. K. C.; Nonappa; Pradeep, T. Interparticle Antigalvanic Reactions of Atomically Precise Silver Nanoclusters with Plasmonic Gold Nanoparticles: Interfacial Control of Atomic Exchange. *Chem. Mater.* **2024**, *36*, 7581–7594

51. Bairagi, D.; Ghosh, P.; Roy, P.; Banerjee, A. Metallogels from Silver Nanoparticles and Peptide Nanofibers as Antimicrobial Surfaces. *ACS Appl. Nano Mater.* **2023**, *6*, 2299–2309.

52. Wang, X.; Fei, Y.; Chen, J.; Pan, Y.; Yuan, W.; Zhang, L. Y.; Guo, C. X.; Li, C. M. Directionally *In situ* Self-Assembled, High-Density, Macropore-Oriented, CoP-Impregnated, 3D Hierarchical Porous Carbon Sheet Nanostructure for Superior Electrocatalysis in the Hydrogen Evolution Reaction. *Small* **2022**, *18*, 2103866.

53. Wang, X.; Fei, Y.; Wang, W.; Yuan, W.; Li, C. M. Polymer-Mediated Self-Assembly of Amorphous Metal–Organic Complexes toward Fabrication of Three-Dimensional Graphene Supported CoP Nanoparticle-Embedded N-Doped Carbon as a Superior Hydrogen Evolution Catalyst. *ACS Appl. Energy Mater*. **2019,** *2*, 8851–8861.

Table of Content